Progress In Electromagnetics Research C, Vol. 75, 1–11, 2017

Electromagnetic Analysis on Propagation Characteristics of CRLH Waveguide Loaded with Double Ridge Corrugations

Qingshan Yang[1, *], Xiaowen Zhao[1], and Yunhua Zhang[1, 2]

Abstract—The propagation characteristics of a composite right/left-handed (CRLH) waveguide loaded with air-filled double ridge corrugations (DRCs) is studied intensively in this paper. It is analyzed from the perspective of electromagnetic (EM) fields other than equivalent circuit method used by many other CRLH structures. First, the EM fields inside the CRLH waveguide are derived theoretically based on the EM fields in the rectangular waveguide and the DRC, as well as the boundary conditions on the interface, respectively. Then the propagation characteristics of the CRLH waveguide including the dispersion relation, surface current and transmitted power are determined according to the EM fields. The properties of the surface current are focused on for analyzing the application possibility of this CRLH waveguide to the leaky-wave antennas (LWAs). The transmitted power of the CRLH waveguide is calculated to demonstrate the high power capacitance of this CRLH waveguide. All the theoretical results are verified through full-wave simulations.

1. INTRODUCTION

Composite right/left-handed (CRLH) transmission line (TL) structures have been studied extensively over the past decades due to their unusual properties such as supporting backward and forward wave propagations simultaneously and infinite wavelength propagation [1]. Numerous CRLH TL structures have been proposed so far, and they can be generally classified into two categories: planar structures [2–10] and three-dimensional (3D) waveguide structures [11–14]. Planar CRLH TLs have the advantages of low profile, low weight, low cost and easy fabrication, etc. They are usually realized using microstrip [2, 3], substrate integrated waveguide (SIW) [4, 6, 7], and ridge substrate integrated waveguide (RSIW) [9, 10], etc. However, they suffer from high loss and low power capacity when operating at the frequency bands above Ku band. Thus this type of CRLH TLs is not suitable for practical radar systems which require high power capacity for long range operation. The waveguide CRLH TLs have higher power capacity than the planar ones, and they may satisfy the actual requirements for radar applications. The CRLH waveguide with dielectric-filled corrugations proposed in [11] has been applied to leaky-wave antennas (LWAs) [15, 16]. However, the radiation efficiency is low due to high dielectric loss, thus this CRLH waveguide with dielectric-filled corrugations is not suitable for high performance LWAs. To avoid the dielectric loss, air-filled CRLH waveguide can be a good choice. A dielectric-free CRLH waveguide LWA consisting of one shorted stub and two twisted H-plane irises in [14] can overcome the dielectric losses. However, the obstacles inside the waveguide cause poor voltage standing wave ratios (VSWRs) of the antenna, let alone the fabrication complexity. So this type of CRLH waveguide is still not suitable for high performance LWAs.

The CRLH waveguide adopted in this paper was first proposed in [13] with the left-handed propagation investigated using full-wave simulation. It is composed of a main rectangular waveguide with one broadwall periodically loaded by air-filled double ridge corrugations (DRCs). This CRLH

Received 22 March 2017, Accepted 27 May 2017, Scheduled 3 June 2017

* Corresponding author: Qingshan Yang (flyangster@gmail.com).

[1] CAS Key Laboratory of Microwave Remote Sensing, National Space Science Center, Chinese Academy of Sciences, China. [2] University of Chinese Academy of Sciences, China.

waveguide has the advantages of high power capacity, low loss and high efficiency, which might be a good choice in practical radar applications. Many CRLH structures proposed before were studied using equivalent circuit method or full-wave simulation. A generalized form of the asymptotic corrugation boundary conditions has been employed to analyze this CRLH waveguide [17]. However, only the dispersion relation is focused on without the propagation characteristics analyzed, which describes the performance of the CRLH waveguide. In this paper, we study the propagation characteristics of this CRLH waveguide from the perspective of electromagnetic (EM) fields other than the equivalent circuit method and discuss the possibility of applying this CRLH waveguide to high performance LWAs.

This paper is organized as follows. The configurations and EM fields of the CRLH waveguide are first derived theoretically in Section 2. Section 3 studies the propagation characteristics of this air-filled CRLH waveguide based on the EM fields deduced in Section 2. In this section, the dispersion relation is first deduced, and the propagation parameters such as phase velocity, group velocity and guided wavelength are calculated. Then the surface current and transmitted power are determined. The properties of the surface current are analyzed in detail to demonstrate the leaky-wave principle when being applied to LWAs. The transmitted power of the CRLH waveguide is also calculated to estimate the power capacitance of this CRLH waveguide. Section 4 gives the comparison of the EM theoretical analysis results and full-wave simulation results, which demonstrates the effectiveness of the EM fields analysis for the propagation characteristic of the CRLH waveguide. Finally, conclusions are drawn.

2. CONFIGURATIONS & EM FIELDS

The unit cell configuration of the CRLH waveguide is shown in Figs. 1(a)–(c). A CRLH waveguide can be realized by periodically cascading the unit cell. Stepped transitions are used in the two ends of the

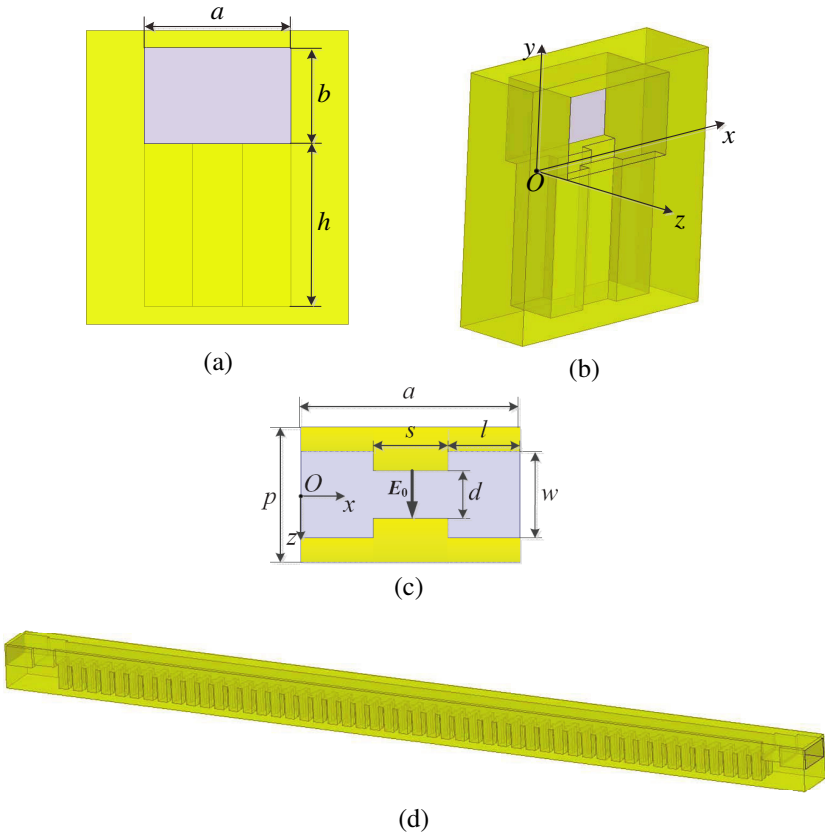

Figure 1. The configurations of the CRLH waveguide. (a) Side view of the unit cell. (b) 3-D view of the unit cell. (c) Top view of the unit cell. (d) Closed CRLH waveguide with input and output stepped transitions.

CRLH waveguide for connecting the structure to standard waveguides, as depicted in Fig. 1(d).

For the interface between the main waveguide and the DRC shown in Fig. 1(c), the boundary conditions are expressed in the following form [17]

$$\iint_{Sp} E_z^w|_{y=0^+} ds = \iint_{Sa} E_z^c|_{y=0^-} ds \tag{1a}$$

$$\iint_{Sp} E_x^w|_{y=0^+} ds = \iint_{Sp} E_x^c|_{y=0^-} ds \tag{1b}$$

$$\iint_{Sa} H_x^w|_{y=0^+} ds = \iint_{Sa} H_x^c|_{y=0^-} ds \tag{1c}$$

where Sa denotes the air aperture surface of the interface, and Sp denotes the whole interface including the conducting and air parts.

Enforcing the boundary conditions on the upper conducting wall of the CRLH waveguide shown in Fig. 1(d), the longitudinal EM fields in the main waveguide can be expressed in the form

$$E_z^w = A_1 E_0 \sin(k_x x) \frac{\sinh(\chi(b-y))}{\sinh(\chi b)} e^{-j\beta z} \tag{2a}$$

$$H_z^w = A_2 \frac{E_0}{\eta_0} \cos(k_x x) \frac{\cosh(\chi(b-y))}{\sinh(\chi b)} e^{-j\beta z} \tag{2b}$$

where β is the propagation constant, k_0 the wave number in free space, and

$$k_x = \pi/a, \quad \chi^2 = k_x^2 - k_{cm}^2, \quad k_{cm}^2 = k_0^2 - \beta^2 \tag{3}$$

The transverse EM fields in the main waveguide then can be deduced as [19]

$$\begin{pmatrix} E_x^w \\ H_y^w \\ H_x^w \\ E_y^w \end{pmatrix} = \frac{-j}{k_{cm}^2} \begin{pmatrix} \omega\mu & \beta & 0 & 0 \\ \beta & \omega\varepsilon & 0 & 0 \\ 0 & 0 & \beta & -\omega\varepsilon \\ 0 & 0 & -\omega\mu & \beta \end{pmatrix} \cdot \begin{pmatrix} \dfrac{\partial H_z^w}{\partial y} \\ \dfrac{\partial E_z^w}{\partial x} \\ \dfrac{\partial H_z^w}{\partial x} \\ \dfrac{\partial E_z^w}{\partial y} \end{pmatrix} \tag{4}$$

The dominant mode field expressions inside the double ridge waveguide are reported in [18]. They are presented as transverse electromagnetic (TEM) mode in the gap, and with some higher order, cutoff transverse magnetic modes in the large parts by matching the electric field at the edge of the ridge to the TEM mode on the gap side. The fields expressions can be found in [17] and [18].

Together with the EM fields inside the main waveguide, as well as the boundary conditions expressed by Eqs. (1a) and (1b), the unknown A_1 in Eq. (2) can be determined as

$$\begin{aligned} A_1 = \frac{k_x \beta}{\sin(\beta p/2)} \Bigg[& \frac{d\cos(k_c s/2)}{w\sin(k_c l)} \cdot (1-\cos(k_c l)) \cdot \frac{\sin(\beta w/2)}{k_c \beta} \\ & + \sum_{n=1}^{\infty} \frac{2w\cos(k_c s/2)\sin(n\pi d/w)}{((n\pi)^2 \sinh(\gamma_n l)} \cdot \frac{\cosh(\gamma_n l)-1}{\gamma_n} \cdot \sin(n\pi/2) + \frac{\sin(k_c s/2)\sin(\beta d/2)}{k_c \beta} \Bigg] \end{aligned} \tag{5}$$

where

$$\gamma_n^2 = (n\pi/w)^2 - k_c^2 \tag{6}$$

Due to the odd symmetry of E_x^c in the DRC, its integral in Eq. (1b) equals zero, thus we have

$$A_2 = \frac{\beta k_x}{k_0 \chi} A_1 \tag{7}$$

and thereby

$$E_x^w = 0 \tag{8}$$

In this way, all the EM field components inside the CRLH waveguide are derived.

3. PROPAGATION CHARACTERISTICS

3.1. Dispersion

Dispersion is one of the most important parameters for the CRLH structure. The left-handed region, right-handed region and stopband region or balanced frequency can be distinguished directly from their dispersion curves. Substituting the EM fields of the CRLH waveguide into the boundary condition of Eq. (1c), we have

$$-\kappa \cdot \coth(\kappa h) = \frac{(1-\cos(k_x l))\sin(\beta w/2) + \cos(k_x l)\sin(\beta d/2)}{\sin(\beta p/2)} \cdot \frac{k_x^2 - k_0^2}{\chi} \coth(\chi b) \tag{9}$$

As can be seen, the unknown variables in both sides of Eq. (9) are the propagation constant β and frequency ω only, thus Eq. (9) is the dispersion relation. Besides, the solution of Eq. (9) is $\chi = 0$ if the depth of the DRC $h \to 0$, which results in

$$\beta = \sqrt{k_0^2 - k_x^2} \tag{10}$$

It is interesting to see that Eq. (10) is the propagation constant of the domain mode (TE_{10} mode) in the traditional rectangular waveguide.

Based on the dispersion relation, the guided wavelength λ_g, phase velocity υ_p and group velocity υ_g can be calculated using Eqs. (11)–(13)

$$\lambda_g = 2\pi/|\beta| \tag{11}$$

$$\upsilon_p = \omega/\beta \tag{12}$$

$$\upsilon_g = \frac{\partial \omega}{\partial \beta} \tag{13}$$

3.2. Surface Current

It is known that the induced current would be generated on the inner wall of the waveguide when microwave signal propagates inside the waveguide. In the microwave frequency, the induced current flows just on the surface of the inner wall because of the skin effect, thus the current can be treated as surface current. The amplitudes and directions of the surface currents are determined by the tangent magnetic fields on the waveguide wall,

$$\mathbf{J}_s = \hat{n} \times \mathbf{H}_{\tan} \tag{14}$$

For the upper broadwall, the surface current is calculated as

$$\begin{aligned} \mathbf{J}_s|_{y=b} &= -\hat{y} \times \mathbf{H}^w_{\tan}|_{y=b} = \hat{z} \cdot H^w_x|_{y=b} - \hat{x} \cdot H^w_z|_{y=b} \\ &= \frac{A_1 E_0 e^{-j\beta z}}{\eta_0 k_0 \chi \sinh(\chi b)} \left[\hat{z} j (k_0^2 - k_x^2)\sin(k_x x) - \hat{x}\beta k_x \cos(k_x x)\right] \end{aligned} \tag{15}$$

The current at the position of $x = 0$,

$$\mathbf{J}_s|_{y=b,x=0} = -\hat{x}\frac{A_1 E_0 e^{-j\beta z}}{\eta_0 k_0 \chi \sinh(\chi b)} \cdot \beta k_x \tag{16}$$

while the current at the position of $x = a$ is,

$$\mathbf{J}_s|_{y=b,x=a} = \hat{x}\frac{A_1 E_0 e^{-j\beta z}}{\eta_0 k_0 \chi \sinh(\chi b)} \cdot \beta k_x \tag{17}$$

and the current at the centerline ($x = a/2$) is,

$$\mathbf{J}_s|_{y=b,x=a/2} = \hat{z}\frac{j A_1 E_0 e^{-j\beta z}}{\eta_0 k_0 \chi \sinh(\chi b)} \cdot (k_0^2 - k_x^2) \tag{18}$$

It is observed from Eqs. (15)–(18) that the surface current distribution is very similar to that of the traditional rectangular waveguide. There are only x components at the two sides of the broadwall

($x = 0$ and $x = a$). Their amplitudes are equal to each other, while their directions are opposite. For the surface current at the centerline ($x = a/2$), there is only z component, thus there is no radiation for the longitudinal slots cut along the centerline of the broadwall. However, the power can be leaked from the longitudinal slot cut on the broadwall with offsets from the centerline since the x components of the surface current can be cut by the slots. Besides, the bigger offset of the slot corresponds to the larger leaky-wave factor in the x component of the surface current since it is $\cos(k_x x)$. This characteristic is very useful for designing high performance CRLH LWAs because the slot offsets can be varied to realize a tapered excitation distribution for achieving low sidelobe levels of radiation patterns. This leaky-wave radiation has been analyzed and demonstrated by full-wave simulation in [20].

For the current at the sidewall surface of the main waveguide ($y \in [0, b]$), we have

$$\begin{aligned}\mathbf{J}_s|_{x=0} &= \hat{x} \times \mathbf{H}^w_{\tan}|_{x=0} = \hat{z} \cdot H^w_y|_{x=0} - \hat{y} \cdot H^w_z|_{x=0} \\ &= -\frac{A_1 E_0 k_x e^{-j\beta z}}{\eta_0 k_0 \chi \sinh(\chi b)} \cdot [\hat{z} j\chi \sinh(\chi(b-y)) + \hat{y}\beta \cosh(\chi(b-y))] \qquad (19a) \\ \mathbf{J}_s|_{x=a} &= -\hat{x} \times \mathbf{H}^w_{\tan}|_{x=a} = -\hat{z} \cdot H^w_y|_{x=a} + \hat{y} \cdot H^w_z|_{x=a} \\ &= -\frac{A_1 E_0 k_x e^{-j\beta z}}{\eta_0 k_0 \chi \sinh(\chi b)} [\hat{z} j\chi \sinh[\chi(b-y)] + \hat{y}\beta \cosh[\chi(b-y)]] \qquad (19b)\end{aligned}$$

It is observed that the surface currents at the two sidewalls are equal to each other, and there are both y component and z component for the sidewall surface current of the CRLH waveguide with DRC, while only y component exists for the sidewall surface current of the traditional waveguides.

For the sidewall surface current of this CRLH waveguide at $y = b$, there is only y component

$$\mathbf{J}_s|_{x=0,y=b} = -\hat{y}\frac{A_1 E_0 k_x \beta}{\eta_0 k_0 \chi \sinh(\chi b)} e^{-j\beta z} \qquad (20)$$

3.3. Transmitted Power

The energy flow density transmitted in the CRLH waveguide with DRCs can be calculated by the Poynting vector as

$$\begin{aligned}\mathbf{S} &= \frac{1}{2}\Re(\mathbf{E}^w \times \mathbf{H}^{w*}) = \frac{1}{2}\Re[\hat{x}(E^w_y H^{w*}_z - E^w_z H^{w*}_y) \\ &\quad +\hat{y}(E^w_z H^{w*}_x - E^w_x H^{w*}_z) + \hat{z}(E^w_x H^{w*}_y - E^w_y H^{w*}_x)] \qquad (21)\end{aligned}$$

Its longitudinal component S_z is the EM power flowing through the unit area of the waveguide cross section, while S_x and S_y are the energy flow densities transmitting along the x and y directions, respectively. Standing waves appear in the x and y directions due to the waveguide walls. Thus the average transmitted power flowing along the CRLH waveguide is given by

$$P = \int_{x=0}^{a}\int_{y=0}^{b} S_z dy dx \qquad (22)$$

The integration limit in y direction is chosen from 0 to b because the DRCs have no contribution to the longitudinal (z direction) power transmission. Thus only the EM fields in the main waveguide need to be considered. In the left-handed region where β, χ and A_2 are all real numbers, the transmitted power can be computed as

$$P_{LH} = \frac{ab}{4} \cdot \frac{A_1^2 E_0^2 \beta(k_0^2 - k_x^2)}{\eta_0 k_0 \chi^2} \cdot \frac{\sinh(2\chi b)/(2\chi b) + 1}{\cosh(2\chi b) - 1} \qquad (23)$$

While in the right-handed region where β is real, χ and A_2 are imaginary numbers, the transmitted power is calculated as

$$P_{RH} = \frac{ab}{4} \cdot \frac{A_1^2 E_0^2 \beta(k_0^2 - k_x^2)}{\eta_0 k_0 \chi^2} \cdot \frac{\sin(j2\chi b)/(j2\chi b) + 1}{\cos(j2\chi b) - 1} \qquad (24)$$

In fact, Eqs. (23) and (24) can be uniformed as Eq. (23).

Table 1. Geometry parameters of the Ka-band CRLH waveguide.

Parameters	a	b	p	w	s	d	h
Value (mm)	4.47	2.8	2.8	1.8	1.2	1	4.75

4. SIMULATION RESULTS

A Ka-band CRLH waveguide with DRCs is built and simulated using full-wave simulation tools to demonstrate the above theoretical analysis. Perfect conductor (PEC) is assumed for the waveguide material. The geometry parameters of the Ka-band CRLH waveguide are given in Table 1.

4.1. Dispersion

Figure 2 gives the dispersion curves of the Ka-band CRLH waveguide calculated according to the theoretical formula of Eq. (9) and HFSS simulation using eigenmode with periodic boundary condition. **Master and slave boundaries are added on the two sides of the CRLH waveguide unit cell for the HFSS simulation, respectively, and the boundary is set to be PEC outside the CRLH waveguide.** Good agreement can be observed. The dispersion curves show that this CRLH waveguide is a balanced CRLH structure with the transition frequency occurring at 33.65 GHz. The corresponding guided wavelength λ_g, phase velocity v_p and group velocity v_g based on the dispersion can also be determined and presented in Fig. 3, Fig. 4 and Fig. 5, respectively. The free space wavelength is plotted in Fig. 3, from which one can find that the guided wavelength is larger than the free space wavelength in the frequency region from 32 GHz to 40 GHz, which means that this frequency region is the fast-wave region. Thus this CRLH waveguide can be applied to antennas with radiating slots cutting on the waveguide surface. The phase velocity given in Fig. 4 exhibits a pole at the transition frequency. On the other hand, for the group velocity in Fig. 5, there is no zero observed between the left-handed region and right-handed region since this CRLH structure is balanced [1].

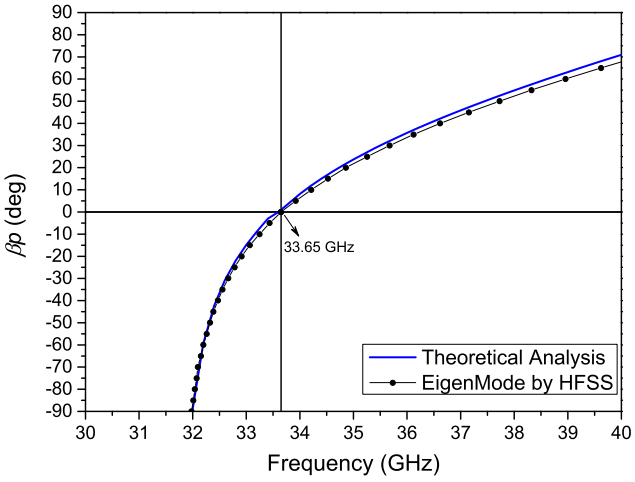

Figure 2. The dispersion relations of the Ka-band CRLH waveguide.

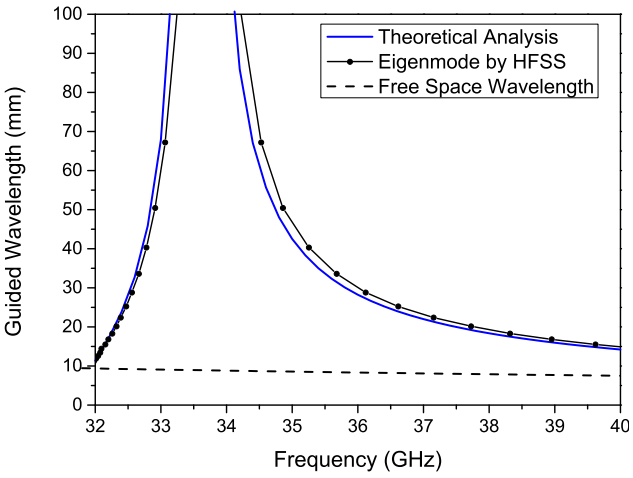

Figure 3. The guided wavelength of the Ka-band CRLH waveguide.

4.2. Surface Current

The upper broadwall surface current of the Ka-band CRLH waveguide is calculated by the theoretical formula of Eq. (15) and plotted in Fig. 6. As comparison, the CRLH waveguide is also simulated using CST Microwave Studio, and the corresponding surface current is given in Fig. 7. They are in

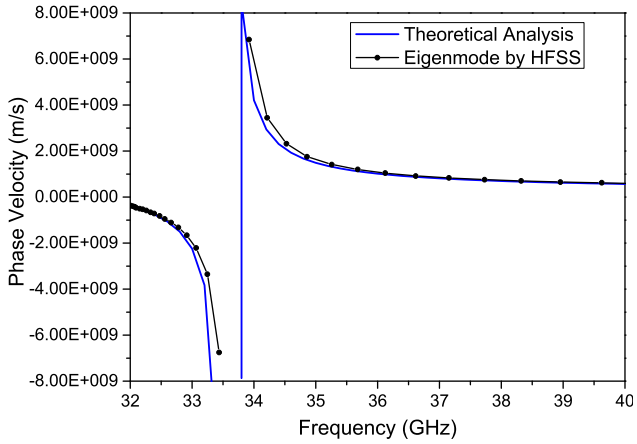

Figure 4. The phase velocity of the Ka-band CRLH waveguide.

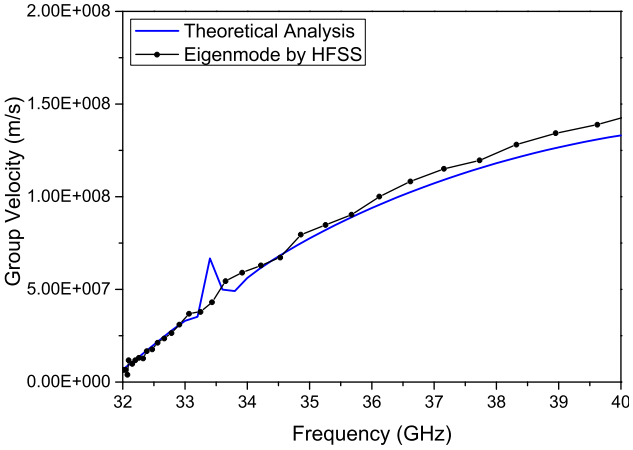

Figure 5. The group velocity of the Ka-band CRLH waveguide.

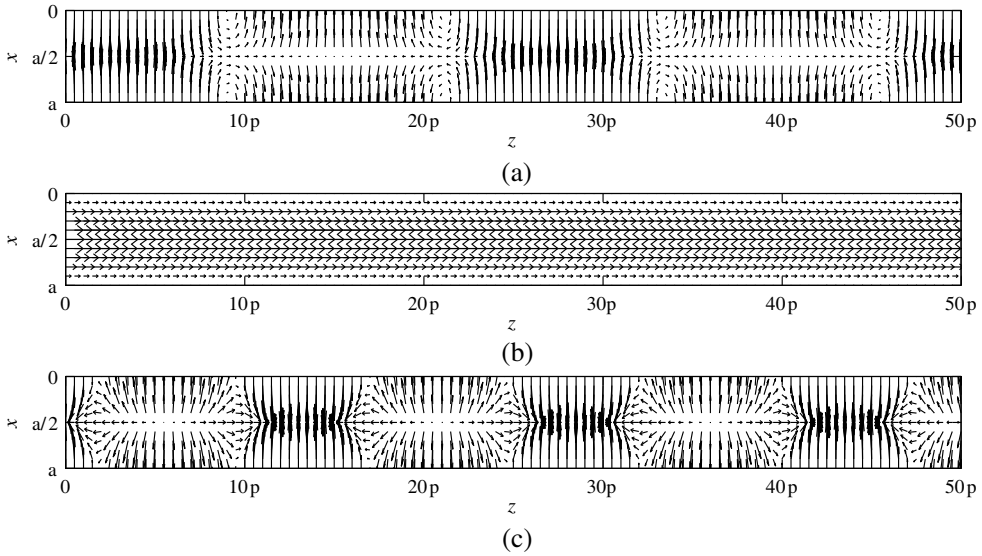

Figure 6. The upper broadwall surface current of the Ka-band CRLH waveguide calculated by the theoretical analysis. (a) $f = 33\,\text{GHz}$, (b) $f = 33.65\,\text{GHz}$, (c) $f = 35\,\text{GHz}$.

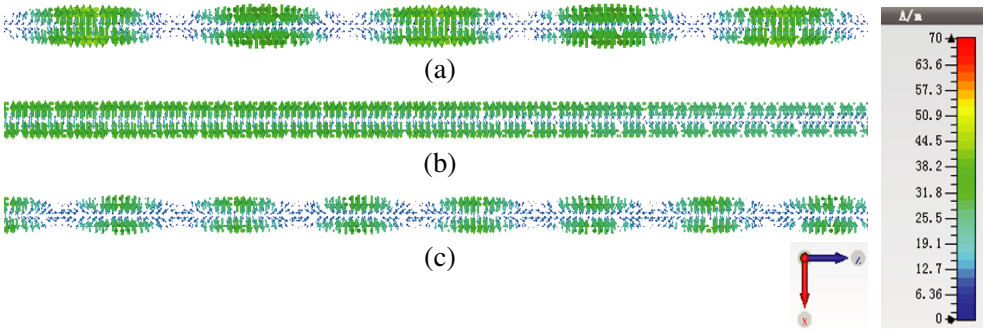

Figure 7. The upper broadwall surface current of the Ka-band CRLH waveguide simulated by CST Microwave Studio. (a) $f = 33\,\text{GHz}$, (b) $f = 33.65\,\text{GHz}$, (c) $f = 35\,\text{GHz}$.

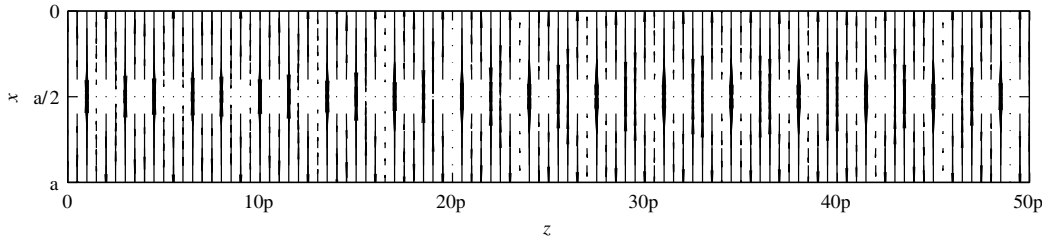

Figure 8. The upper broadwall surface current of the Ka-band CRLH waveguide at 33.7 GHz (near the transition frequency).

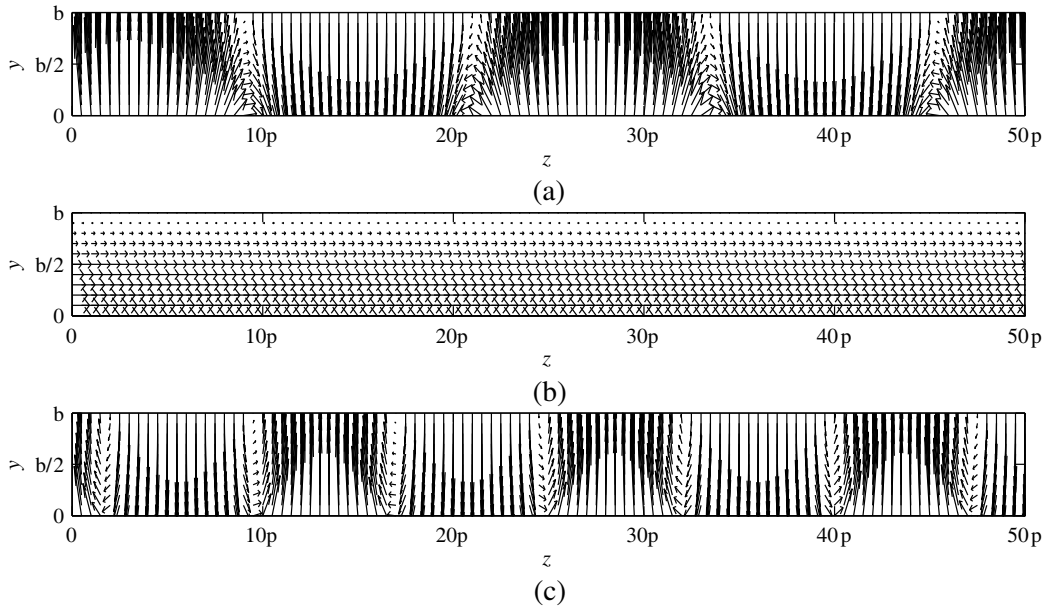

Figure 9. The sidewall surface current of the Ka-band CRLH waveguide calculated by theoretical analysis. (a) $f = 33$ GHz, (b) $f = 33.65$ GHz, (c) $f = 35$ GHz.

accordance with each other for the frequencies at 33 GHz (left-handed region) and 35 GHz (right-handed region), and they both show similar surface current distribution on the broadwall to that of traditional waveguide, as concluded by Eq. (15). Only x components are observed at the two sides of the broadwall ($x = 0$ and $x = a$) while at the centerline ($x = a/2$), there is only z component. It is interesting to find that different surface current distributions are exhibited at the transition frequency of 33.65 GHz in Fig. 6 and Fig. 7. In Fig. 6, there is only z direction surface current, while both x and z direction surface currents are observed in Fig. 7. This is because the propagation constant β equals zero strictly in the theoretical analysis, while in the actual prototype simulation, the strict zero propagation constant (or the strict balanced condition) is usually hard to achieve [5, 10]. Furthermore, the surface current at 33.7 GHz, which is near the transition frequency, has also been analyzed theoretically and plotted in Fig. 8. It is in accordance with the current distribution in Fig. 7(b).

The sidewall surface current of the Ka-band CRLH waveguide is also calculated using Eq. (19) and given in Fig. 9. Fig. 10 shows the corresponding surface current distribution simulated by CST Microwave Studio for comparison. Unlike the traditional waveguide, there are both y and z components for the sidewall surface current of the CRLH waveguide in both the left-handed and right-handed regions. Only y component is observed when $y = b$, as discussed in Section 3.2. The different surface current distributions also occur at the transition frequency between Fig. 9(b) and Fig. 10(b) because of the same reason as discussed above. The sidewall surface current at 33.7 GHz (near the transition frequency) plotted in Fig. 11 shows agreement with that in Fig. 10(b).

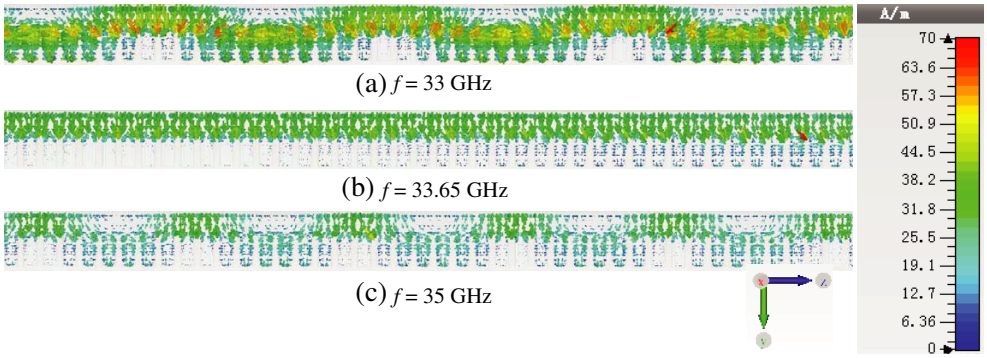

Figure 10. The sidewall surface current of the Ka-band CRLH waveguide simulated by CST Microwave Studio. (a) $f = 33\,\text{GHz}$, (b) $f = 33.65\,\text{GHz}$, (c) $f = 35\,\text{GHz}$.

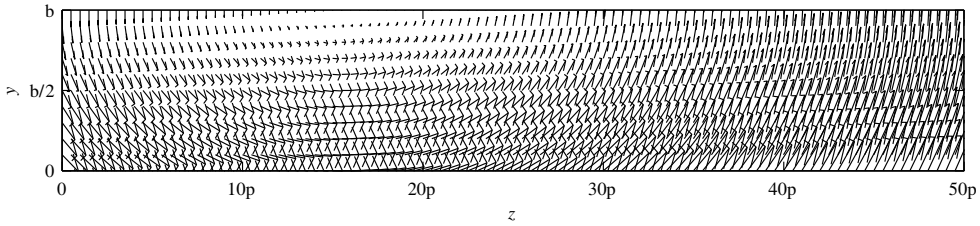

Figure 11. The sidewall surface current of the Ka-band CRLH waveguide at 33.7 GHz (near the transition frequency).

4.3. Transmitted Power

Taking $E_{br} = 3000\,\text{kV/m}$ as the breakdown field strength of air, the peak power capacitance of the CRLH waveguide can be calculated by Eq. (22) and plotted in Fig. 12. As predicted, high power capacitance of this air-filled CRLH waveguide is shown, and this characteristic makes the CRLH waveguide more suitable for the practical radar application than the planar CRLH structures. As we all know, in radar application, the operation range is decided mainly by the transmitted power, antenna gain, and sensitivity of the receiver according to the radar equation if some radar cross-section (RCS) is assumed. Higher transmitted power is very helpful for longer operation range. Thus an LWA based on this CRLH waveguide can be a better choice than the planar LWAs for radar application.

It should be noted that a zero exhibits at the transition frequency in Fig. 12. This can be explained

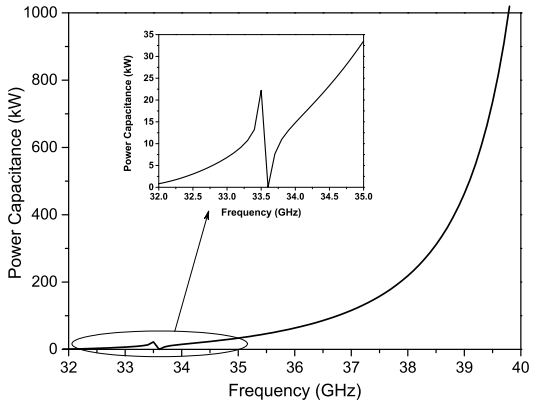

Figure 12. The power capacitance of the air-filled CRLH waveguide.

as that the electric length of the CRLH waveguide at the transition frequency is zero, and the EM waves inside the waveguide can be considered as standing wave with the EM power transmitted only in the x and y directions. Besides, from the point of view of the energy flow, although the Poynting vector can be considered as the EM energy flow density, it is not rigorous since it is $\nabla \cdot \mathbf{S}$ that represents the variation of the energy density other than the Poynting vector itself according to the Poynting's theorem. The $\nabla \cdot \mathbf{S}$ in the z direction at the transition frequency equals zero, which also indicates the EM power transmitting only in the x and y directions. Therefore, Eq. (22) is not appropriate for the power calculation at the transition frequency.

5. CONCLUSION

The propagation characteristics of the CRLH waveguide loaded with air-filled DRCs are studied through EM analysis. The EM fields inside the CRLH waveguide are derived based on the EM fields in the rectangular waveguide and the DRC, as well as the boundary conditions on the interface. An implicit expression for the dispersion relation of this CRLH waveguide is derived. The comparison of the dispersion results between the theoretical analysis and the full-wave simulation verifies the derived formulae.

The surface currents on the upper broadwall and the sidewall of the CRLH waveguide are focused on. The current on the upper broadwall shows similar distribution to that of the traditional rectangular waveguide, while different distributions are shown for the surface currents between the sidewalls of the CRLH waveguide and traditional waveguide. They are both verified by the theoretical analysis and full-wave simulation. The calculated high power capacitance of this CRLH waveguide demonstrates that it is more suitable for practical radar applications than the planar CRLH structures.

The propagation characteristics of this CRLH waveguide show potential application to the high performance LWAs with high power capacitance, low loss and high radiation efficiency. Long longitudinal slots may be cut on the upper broadwall to realize the LWA. Continuous beam-steering capabilities from backfire to endfire including the broadside direction can be achieved by the balanced CRLH waveguide LWA. Besides, the sidelobe level of the antenna patterns can be more conveniently optimized by using meandering long slots compared with the planar CRLH LWAs.

ACKNOWLEDGMENT

This work was supported in part by the National Natural Science Foundation of China under Grant 61501432 and by the Youth Innovation Promotion Association of Chinese Academy of Sciences under Grant 2017189.

REFERENCES

1. Caloz, C. and T. Itoh, *Electromagnetic Metamaterials: Transmission Line Theory and Microwave Applications: The Engineering Approach* /, Wiley-IEEE Press, 2006.
2. Liu, L., C. Caloz, and T. Itoh, "Dominant mode leaky-wave antenna with backfire-to-endfire scanning capability," *Electron. Lett.*, Vol. 38, No. 23, 1414–1416, 2002.
3. Abdelaziz, A. F., T. M. Abuelfadl, and O. L. Elsayed, "Realization of composite right/left-handed transmission line using coupled lines," *Progress In Electromagnetics Research*, Vol. 92, 299–315, 2009.
4. Dong, Y. and T. Itho, "Composite right/left-Handed substrate integrated waveguide and half mode substrate integrated waveguide leaky-wave structures," *IEEE Trans. Antennas Propag.*, Vol. 59, No. 3, 767–775, 2011.
5. Dong, Y. and T. Itho, "Substrate integrated composite right-/left-handed leaky-wave structure for polarization-flexible antenna application," *IEEE Trans. Antennas Propag.*, Vol. 60, No. 2, 760–771, 2012.

6. Yang, Q., Y. Zhang, and X. Zhang, "X-band composite right/left-handed leaky wave antenna with large beam scanning-range/bandwidth ratio," *Electron. Lett.*, Vol. 48, No. 13, 746–747, 2012.
7. Yang, Q., Y. Zhang, and X. Zhang, "A shunt-capacitance-aided composite right/left-handed leaky wave antenna with large scanning-range/bandwidth ratio," *PIERS Proceedings*, 649–652, Moscow, Russia, Aug. 19–23, 2012.
8. Yang, T., P.-L. Chi, and R.-M. Xu, "Novel composite right/left-handed leaky-wave antennas based on the folded substrate-integrated-waveguide structures," *Progress In Electromagnetics Research C*, Vol. 29, 235–248, 2012.
9. Yang, Q. and Y. Zhang, "Non-radiative composite right/left-handed transmission line based on ridge substrate integrated waveguide," *Electron. Lett.*, Vol. 49, No. 20, 1280–1282, 2013.
10. Yang, Q., X. Zhao, and Y. Zhang, "Composite right/left-handed ridge substrate integrated waveguide slot array antennas," *IEEE Trans. Antennas Propag.*, Vol. 62, No. 4, 2311–2316, 2014.
11. Eshrah, I. A., A. A. Kishk, A. B. Yakovlev, and A. W. Glisson, "Rectangular waveguide with dielectric-filled corrugations supporting backward waves," *IEEE Trans. Microw. Theory Tech.*, Vol. 53, No. 11, 3298–3304, 2005.
12. Chen, Y., S.-W. Liao, J. Wei, and J.-H. Xu, "Unequally spaced and excited resonant slotted-waveguide antenna array based on an improved resonant-slot coupled cavity chain composite right/left-handed waveguide," *Progress In Electromagnetics Research*, Vol. 110, 421–435, 2010.
13. Eldeen, A. M. N. and I. A. Eshrah, "CRLH waveguide with air-filled double-ridge corrugations," *Proc. IEEE Symp. Antennas Propag. Soc. Int. Symp.*, 2965–2968, Spokane, Washington, USA, 2011.
14. Kim, D. J. and J. H. Lee, "Beam scanning leaky-wave slot antenna using balanced CRLH waveguide operating above the cutoff frequency," *IEEE Trans. Antennas Propag.*, Vol. 61, No. 5, 2432–2440, 2013.
15. Navarro-Tapia, M., J. Esteban, and C. Camacho-Pealosa, "Initial assessment of a waveguide with dielectric-filled corrugations as a technology for slot antennas with backward-to-forward scanning capabilities," *Metamaterials*, Vol. 3, 174–184, 2009.
16. Navarro-Tapia, M., J. Esteban, and C. Camacho-Pealosa, "On the actual possibilities of applying the composite right/left-handed waveguide technology to slot array antennas," *IEEE Trans. Antennas Propag.*, Vol. 60, No. 5, 2183–2193, 2012.
17. Kord, A. M. and I. A. Eshrah, "Generalised asymptotic boundary conditions and their application to composite right/left-handed rectangular waveguide with double-ridge corrugations," *IET Microw. Antennas Propag.*, Vol. 8, No. 13, 1014–1020, 2014.
18. Getsinger, W. J., "Ridge waveguide field description and application to directional couplers," *IRE Trans. Microw. Theory Tech.*, Vol. 10, 41–50, 1962.
19. Yang, Q., X. Zhao, and Y. Zhang, "CRLH waveguide based Ka-band beam-steering leaky-wave antenna for radar application," *PIERS Proceedings*, 2820–2823, Prague, Jul. 6–9, 2015.
20. Yang, Q., X. Zhao, and Y. Zhang, "Leaky-wave radiation analysis for CRLH waveguide with long slot on its broadwall," *2016 10th European Conference Antennas Propag. (EuCAP2016)*, Davos, Switzerland, 2016.